Characterization of the Reaction Products of Laser-Ablated Lanthanide Metal Atoms with Nitric Oxide. Infrared Spectra of the NLnO Molecules in Solid Argon†

Stephen P. Willson and Lester Andrews*
Department of Chemistry, University of Virginia, Charlottesville, Virginia 22901

Matthew Neurock
Department of Chemical Engineering, University of Virginia, Charlottesville, Virginia 22901

Received: August 4, 1999; In Final Form: November 18, 1999

This paper reports stretching frequencies of the novel NLnO lanthanide nitride, oxide molecules and the $NCeO^-$ and $NPrO^-$ anions in solid argon. Combination bands observed for NCeO, NPrO, NNdO, and NTbO confirm these assignments, and density functional calculations are presented to model the vibrational potentials of NCeO, NPrO, NNdO, NGdO, NTbO, and NLuO. The Ln−O frequencies of the NLnO molecules range from 800 to 720 cm^{-1}, except for the case of NEuO, which is lower, near the EuO diatomic molecule. The Ln−N frequencies of the NLnO molecule depend on the availability of electrons for the LnN bond after the LnO double bond has been satisfied and, therefore, suggest the presence of three different bond orders, depending on the metal center. In NLuO, the Lu−N mode is 425.6 cm^{-1}, and the Lu atom retains a filled f-shell; the Ce−N bond of NCeO has a higher frequency, 690.8 cm^{-1}, and NPrO has a Pr−N mode at 900.8 cm^{-1}, which is even higher than the PrN diatomic mode (857.9 cm^{-1}). In addition, NO complexes with Ln, LnO, and CeO_2 have been identified. The increase in yield of these complexes and NLnO insertion products on annealing may be useful in the development of models for the catalytic activity of Ln atoms in the conversion of NO to N_2.

Introduction

A significant environmental problem facing industrial nations today is the production of noxious gases, particularly from the widespread combustion of fossil fuels. One of the more insidious pollutants is nitric oxide, present in emissions from automobile exhausts. Catalytic conversion of NO to N_2 is therefore a matter of intense practical and scientific concern, and there has been a considerable amount of effort expended in this pursuit. Today, a variety of catalysts are available for this purpose, and the search continues for more efficient materials.

Over 20 years ago, it was shown that, with CO present, CeO_2 catalytically reduces NO, with similar activity to platinum and palladium catalysts.[1] Recent studies show that the inclusion of lanthanide metals and oxides in copper-based zeolites, used for the selective catalytic reduction of NO, enhances the activity of the catalysts.[2−4] The most commonly used lanthanide for this purpose is cerium, although samarium and europium also yield promising results.[2,5] Zeolites containing Ce and Ag catalyze the reduction of NO by CH_4 in excess O_2,[6] and oxides containing La and Ce or Eu catalyze reduction of NO by H_2.[5] In addition, NO has been shown to dissociatively adsorb on polycrystalline gadolinium.[7]

Owing to the absence of data for the simple lanthanide−nitric oxide triatomics or small nitrosyls, the abundance of which may lead to a deeper understanding of the function of lanthanide elements in the selective catalytic reduction of NO, we have undertaken this study to identify the reaction products and intermediates of laser-ablated lanthanide atoms with nitric oxide. It is interesting to note that nearly all lanthanide metals insert into the NO bond to form NLnO molecules upon the annealing of argon matrixes containing atomic Ln and NO, that is, the insertion occurs without an activation energy. The same cold insertion reaction with NO has been observed for Sc, Ti, and V atoms[8,9] and the third-row analogues La, Hf, and Ta.[10,11] Additionally, the formation of the side-bound Ln(NO) complex also proceeds spontaneously in several instances and continues to insertion with the assistance of UV photons.

Prior theoretical work on small molecules containing a lanthanide metal atom has successfully modeled Ln interactions with O by appeal to the ligand field.[12] A significant body of theoretical and experimental literature is available pertaining to the LnO diatomic molecules described in the context of $Ln^{2+}O^{2-}$.[13,14] This study provides a foothold on the complex electronic structure of atomic Ln in the simultaneous ligand fields of both N and O and compares experimental results obtained for the NLnO molecules, which have both Ln−N and Ln−O stretching modes, with previous descriptions of LnO,[13] OLnO,[13] and LnN[15] species, to provide information on the electronic configurations.

Experimental Section

Lanthanide metal atoms, supplied by laser vaporization of metal targets, were reacted with nitric oxide in argon matrices using techniques described in previous publications.[16,17] The experiments required NO concentrations in argon ranging from 0.2 to 0.4%, deposited at a rate of 4−5 mmol/h for 45−75 min onto a CsI window maintained at 6−7 K. Samples of $^{15}N^{16}O$, mixed $^{14}N^{16}O + {}^{15}N^{16}O$, $^{15}N^{18}O$, and mixed $^{15}N^{16}O + {}^{15}N^{18}O$ were also employed ($^{14}N^{16}O$, Matheson; $^{15}N^{16}O$, MDS Isotopes, 99%; $^{15}N^{18}O$, Isotec, 99%). To identify charged products, some gas samples were doped with 0.05% CCl_4. Infrared spectra were recorded at 0.5 cm^{-1} resolution with a Nicolet 550 spectrometer after deposition and after each annealing or photolysis.

† Part of the special issue "Marilyn Jacox Festschrift".

10.1021/jp992727j CCC: $19.00
Published on Web 01/21/2000

TABLE 1: Product Absorptions (cm^{-1}) Observed for Laser-Ablated Ce Atoms with NO in Solid Argon

^{14}NO	^{15}NO	$^{14}NO + {}^{15}NO$	ratio[a]	$^{15}N^{18}O$	ratio[b]	anneal.[c]	ident
3608.4	3545.2	3608.5, 3579.8, 3545.3	1.0178	3450.5	1.0274	a+0	*c*-$(NO)_2$ combo
1871.6	1838.8	1871.6, 1838.7	1.0178	1789.2	1.0277	a− −	NO
1863.3	1830.4	1863.2, 1849.6, 1830.4	1.0180	1781.1	1.0277	a+0	*c*-$(NO)_2$
1776.1	1744.6	1776.1, 1757.5, 1744.6	1.0181	1697.4	1.0278	a+0	*c*-$(NO)_2$
1688.5	1660.3		1.0170			a0−(+)	N_2O_3
1589.3	1562.0	1589.1, 1574.8, 1561.7	1.0175	1520.1	1.0276	a+ −(−)	$(NO)_2^+$
1583.3	1555.8	1583.2, 1568.9, 1555.8	1.0177	1514.3	1.0274	a+ −(−)	$(NO)_2^+$ site
1510.2	1499.1	1510.3, 1499.2	1.0074	1451.0	1.0331	a+ −	NCeO overtone
1498.3	1472.2	1498.9, 1483.5, 1471.5	1.0177	1433.0	1.0274	b+	(η^1-$NO)_2CeO_2$
1444.4	1423.7	1444.5, 1423.7	1.0145	1384.6	1.0282	a+ −	NCeO combo
1392.4	1358.1	1392.4, 1364.9, 1358.0	1.0253	1340.3	1.0133	b+(−)	(η^1-$NO)_2$Ce
1341.1	1318.4	1341.2, 1318.4	1.0172	1281.8	1.0286	b+(−)	(η^1-NO)Ce
1300.2	1278.9	1300.2, 1291.2, 1278.9	1.0167	1242.7	1.0291	a− −	*c*-$(NO)_2^-$
1246.4	1221.0		1.0208	1194.7	1.0220	a0−	NO_2^- site
1243.4	1218.1	1243.4, 1218.2	1.0208	1191.8	1.0221	a0−	NO_2^-
1228.0	1203.8	1228.1, 1214.5, 1203.9	1.0201	1177.1	1.0227	a+0(−)	*c*-$(NO)_2^-$ site
1222.6	1198.6	1222.6, 1209.3, 1198.6	1.0200	1172.0	1.0227	a− −(+)	*c*-$(NO)_2^-$
1220.9	1199.8	1220.9, 1209.3, 1199.7	1.0176	1167.3	1.0278	a− −(+)	t−$(NO)_2^-$
1205.3						c−	NNO_2^-
1145.2	1126.0	1145.3, 1126.0	1.0171	1095.6	1.0277	a+0	(η^2-NO)CeO
1078.7	1061.1	1078.7, 1068.8, 1061.1	1.0165	1031.3	1.0289	a++	(η^2-$NO)_2$Ce
911.4	883.5	911.1, 883.7	1.0316	883.7	1.000	b+(+)	? CeN^+ ?
884.3	866.0	884.4, 875.5, 865.9	1.0211	847.7	1.0216	a− −(+)	*c*-$(NO)_2^-$
849.7	849.5	849.7	1.0002	849.6, 806.1	1.0540	a+ −(−)	CeO^+
843.2	817.5	843.2, 817.5	1.0314	817.5	1.000	a+ −	CeN
808.2	808.2	808.2	1.0000	808.2, 767.1	1.0536	a− −(−)	CeO
800.8	800.9	800.8	1.0000	800.9, 760.2	1.0535	a− −	CeO site
770.4	770.4	770.4	1.0000	770.3, 731.7	1.0528	a+0	(η^2-NO)CeO
757.2	751.9	757.2, 751.9	1.0070	727.3	1.0338	a+ −	NCeO
752.3	747.5	- - -, 747.5	1.0064	722.3	1.0349	b+	NCeO site
736.7	736.7	736.7	1.0000	736.7, 701.7	1.0499	a+ −	CeO_2
734.2	734.2	734.2	1.0000	699.3	1.0499	a++	(η^1-NO)CeO_2
732.0	731.9	732.0	1.0001	697.1	1.0501	b+	(η^1-$NO)_2CeO_2$
727.6	727.4	727.5	1.0003	692.8	1.0501	b+	(η^1-$NO)_2CeO_2$ site
690.8	673.9	690.8, ---	1.0251	661.2	1.0192	a+ −	NCeO
676.0	661.2	675.9, 661.2	1.0224	652.0	1.0141	a+ −	Ce(NO)Ce ring
624.8	624.2	624.6	1.0010	593.9	1.0510	a0−(−)**	$NCeO^-$
603.2	594.5	603.1, 602.0, 595.5, 594.6	1.0146	579.1	1.0266	a++(+)	$(NO)_x(NO)_yCeO_z$
520.6	517.1	520.6, 517.1	1.0068	495.7	1.0432	a+ −	Ce(NO)Ce ring

[a] Ratio of $^{14}N^{16}O/^{15}N^{16}O$ isotopic frequencies. [b] Ratio of $^{15}N^{16}O/^{15}N^{18}O$ isotopic frequencies. [c] Annealing behavior: a denotes presence on deposition, +, −, or 0 indicates the direction of growth in two successive annealings, b denotes appearance on the first annealing and +, −, or, 0 indicates changes on second annealing, (+ or −) indicates changes on photolysis, c denotes appearance on photolysis. *Indicates an increase with CCl_4 on deposition. **Indicates a decrease with CCl_4 on deposition.

The metal targets, Ce (99.99%), Pr−Lu (Johnson−Matthey 99.9%), were ablated with the 1064 nm fundamental of a YAG laser, typically with 5−50 mJ pulses. For low laser power experiments, a 10% transmitting neutral density filter was placed in the laser beam. Following deposition, argon matrices, were annealed to 20−25 K, and then subjected to UV photolysis using a 175 W mercury street lamp (Philips H39KB) without the globe (240−580 nm). Alternately, matrices were subjected to a series of photolyses including a tungsten lamp (Sylvania 2518, FCS 24 V), glass filters, and a mercury arc lamp.

Results

Absorptions observed for the laser-ablated lanthanide metal atom and nitric oxide reaction systems fall into two broad categories, those identified as N−O vibrations and those due to Ln−O and Ln−N motions. N−O vibrations range from the NO fundamental at 1871.8 cm^{-1} to the Ln(NO) rings found as low as 700 cm^{-1}. The dimer $(NO)_2$ and the $(NO)_2^+$, $(NO)_2^-$, and NO_2^- ions[9,17,18] were observed in all 13 systems but are listed only for Ce in Table 1. The metal−oxygen and metal−nitrogen fundamentals range from 400 to 1000 cm^{-1}, and absorption bands for each metal are listed with their $^{15}N^{16}O$ and $^{15}N^{18}O$ isotopic counterparts and annealing behavior in Tables 1−13 (radioactive Pm not done). The differences observed after photolysis or with CCl_4 doping are also included with the annealing data. Examples of important spectral regions are provided in Figures 1−6 for clarification of the text.

Calculations

Theoretical calculations were performed for several lanthanide nitroxide species with the Amsterdam Density Functional (ADF 2.1) program, developed by Baerends et al. to aid in making vibrational assignments.[19−21] Exchanges and correlations were accounted for using the Vosko, Wilk, and Nusair parametrized local density approximation,[22] with nonlocal exchange and correlation corrections handled by the Becke and Perdew method (BP86).[23,24] The numerical integration parameter was set to 6.0, which is expected to provide reasonably accurate geometries and vibrational frequencies.[21] The basis sets were triple-ζ, with one polarization function included for the O and N atoms, but without polarization functions for the Ln metal atoms (ADF 2.1, Basis Set IV). The Ln atoms were frozen through the 4d level, and the O and N atoms were frozen through the 1s level. First-order relativistic scalar corrections and diagonalization in the nonrelativistic basis yielded quasi-relativistic solutions.[25,26] The computational results are provided in Table 14 for metals in which convergence was obtained for the states which

TABLE 2: Product Absorptions (cm^{-1}) Observed for Laser-Ablated Pr Atoms with NO in Solid Argon

^{14}NO	^{15}NO	$^{14}NO + {}^{15}NO$	ratio[a]	$^{15}N^{18}O$	ratio[b]	anneal.[c]	ident
1830.5	1798.5	unclear	1.0178	1752.9	1.0260	b+(−)	$(\eta^1\text{-NO})_x\text{Pr}$
1818.8	1786.8	unclear	1.0179	1739.0	1.0275	b+(−)**	$(\eta^1\text{-NO})_x^-\text{Pr}$
1712.0	1681.6	1712.0, 1694.6, 1681.6	1.0181	1636.6	1.0275	b+(−)**	$(\eta^1\text{-NO})_2^-\text{Pr}$
1638.3	1610.9	1638.2, 1610.8	1.0170	1610.8, 1573.1	1.0240	a+ −	NPrO combo
1545.2	1517.9	1545.2, 1530.1, 1518.0	1.0180	1477.5	1.0273	b+*	$(\eta^1\text{-NO}^+)\text{Pr}$
1480.3	1470.7	1480.4, 1470.8	1.0065	1404.8	1.0469	a+ −	NPrO overtone
1416.6	1416.6	1416.6	1.0000	1344.5	1.0536	b+(+)	$(\eta^1\text{-NO})\text{PrO}_2$
1359.3	1335.9	1359.3, 1335.8	1.0175	1299.5	1.0279	a+ −	$(\eta^1\text{-NO})\text{Pr}$
900.8	879.1	900.8, 879.1	1.0247	879.1, 873.0	1.0070	a+ −(+)	NPrO
893.8	872.5	893.7, 872.5	1.0244	866.2	1.0073	a++	NPrO site
867.7	849.2	867.6, 849.2	1.0218	840.8	1.0100	a++(−)	$(\eta^1\text{-NO})_x\text{NPrO}$
857.9	831.6	857.8, 831.7	1.0316	831.7	1.0000	a+ −	PrN
816.7	816.7	816.7	1.000	774.9	1.0539	a0−(−)	PrO
783.0	783.0	783.0	1.000	783.0, 742.9	1.0540	a++(−)	$(\eta^2\text{-NO})\text{PrO}$
742.0	737.0	742.0, 737.0	1.0068	737.0, 703.9	1.0470	a+ −(+)	NPrO
734.7		734.7		697.7		a++(−)	$(\eta^1\text{-NO})_x\text{NPrO}$
730.2	730.1	730.2	1.0000	696.1	1.0490	a+0	OPrO
727.1	727.2	727.1	1.0000	693.5	1.0484	a+ −(+)	$(\eta^1\text{-NO})\text{OPrO}$
718.2	696.5	718.2, 696.5	1.0312			a− −	NPrO^-
677.0	662.7	677.2, 662.8	1.0216	653.8	1.0136	a+ −(+)	?
612.3	612.2	612.2	1.0002	581.3	1.0532	a− −	NPrO^-
520.3	516.8	518.3	1.0068	495.1	1.0438	a0−(−)	Pr(NO)Pr ring

[a] Ratio of $^{14}N^{16}O/^{15}N^{16}O$ isotopic frequencies. [b] Ratio of $^{15}N^{16}O/^{15}N^{18}O$ isotopic frequencies. [c] Annealing behavior: a denotes presence on deposition, +, −, or 0 indicates the direction of growth in two successive annealings, b denotes appearance on the first annealing and +, −, or, 0 indicates changes on second annealing, (+ or −) indicates changes on photolysis, c denotes appearance on photolysis. *Indicates an increase with CCl_4 on deposition. **Indicates a decrease with CCl_4 on deposition.

TABLE 3: Product Absorptions (cm^{-1}) Observed for Laser-Ablated Nd Atoms with NO in Solid Argon

^{14}NO	^{15}NO	$^{14}NO + {}^{15}NO$	ratio[a]	$^{15}N^{18}O$	ratio[b]	anneal.[c]	ident
1424.1	1402.9	1424.1, 1402.9	1.0151	1366.3	1.0268	a+ −	NNdO combo
853.2	827.1	853.2, 827.0	1.0316	827.2	0.9999	a+ −	NdN
814.1	814.1	814.1	1.0000			a0−	NdO
781.4	781.4	781.4	1.0000			a+0	$(\eta^2\text{-NO})\text{ NdO}$
768.7	759.9	768.7, 759.9	1.0116	740.3	1.0265	a+ −	NNdO
716.7	716.7	716.6	1.000	683.6	1.0484	a+ −	ONdO
712.7	712.6	712.7	1.000	679.7	1.0484	b+	$(\eta^1\text{-NO})_x\text{ ONdO}$
661.4	648.6	661.4, 648.6	1.0197	631.5	1.0271	a+ −	NNdO
597.0	596.9	596.9	1.0002	566.2	1.0542	a− −	$(\text{NdO})_2$
525.4	521.3	523.9	1.0079	499.5	1.0436	a+ −	Nd(NO) Nd ring

[a] Ratio of $^{14}N^{16}O/^{15}N^{16}O$ isotopic frequencies. [b] Ratio of $^{15}N^{16}O/^{15}N^{18}O$ isotopic frequencies. [c] Annealing behavior: a denotes presence on deposition, +, −, or 0 indicates the direction of growth in two successive annealings, b denotes appearance on the first annealing and +, −, or, 0 indicates changes on second annealing, (+ or −) indicates changes on photolysis, c denotes appearance on photolysis. *Indicates an increase with CCl_4 on deposition. **Indicates a decrease with CCl_4 on deposition.

TABLE 4: Product Absorptions (cm^{-1}) Observed for Laser-Ablated Sm Atoms with NO in Solid Argon

^{14}NO	^{15}NO	$^{14}NO + {}^{15}NO$	ratio[a]	$^{15}N^{16}O + {}^{15}N^{18}O$	ratio[b]	anneal.[c]	ident
1510.6	1483.3	1510.6, 1495.4, 1483.3	1.0184	1483.4, 1461.2, 1445.3	1.0264	b+(−)	$(\eta^1\text{-NO})_2\text{Sm}$
1186.5	1163.6	1186.5, 1163.6	1.0197			b+	$\text{Sm}^+(\text{NO}_2)^-$
822.7	797.5	822.7, 797.6	1.0316	797.6	1.000	a+ −	SmN
808.1	808.1	808.1	1.0000	808.1, 767.2	1.0533	a0−	SmO
736.9	728.0	736.9, 728.0	1.0122	728.0, 709.4	1.0262	a0−(+)	NSmO
690.7	673.5	690.7, 673.6	1.0255	673.6, 666.9	1.0100	a+ −(+)	?
686.4	666.2	686.4, 666.2	1.0303	- - -, 662.0	1.0063	a− −	?
643.2	643.2	643.2	1.0000	643.2, 633.9, 613.3	1.0488	a++	SmO_2
604.8	593.3	604.8, 593.3	1.0194	593.3, 577.4	1.0275	a+ −(+)	?
531.7	528.2	531.5, 528.2	1.0066	528.2, 509.3	1.0371	a++	?
510.0	497.3	510.0, 497.3	1.0255	497.2, 491.9	1.0108	a− −(+)	?

[a] Ratio of $^{14}N^{16}O/^{15}N^{16}O$ isotopic frequencies. [b] Ratio of $^{15}N^{16}O/^{15}N^{18}O$ isotopic frequencies. [c] Annealing behavior: a denotes presence on deposition, +, −, or 0 indicates the direction of growth in two successive annealings, b denotes appearance on the first annealing and +, −, or, 0 indicates changes on second annealing, (+ or −) indicates changes on photolysis, c denotes appearance on photolysis. *Indicates an increase with CCl_4 on deposition. **Indicates a decrease with CCl_4 on deposition.

appropriately modeled the observed frequencies. In the future, better calculations will be needed for these systems.

Discussion

The primary reaction product of laser-ablated lanthanide metal atoms with nitric oxide is NLnO. The ablated metal atoms form an energized intermediate that is relaxed by the matrix to give the most stable product molecules, the insertion product and the decomposition products, all of which are observed (reaction 1). Alternately, the inserted product can be formed by the ultraviolet photolysis of the Ln(NO) ring addition product, which might be an intermediate for metal insertion into the NO bond

TABLE 5: Product Absorptions (cm^{-1}) Observed for Laser-Ablated Eu Atoms with NO in Solid Argon

^{14}NO	^{15}NO	$^{14}NO + {}^{15}NO$	ratio[a]	$^{15}N^{18}O$	ratio[b]	anneal.[c]	ident
1348.0	1324.7	1348.0, 1328.7, 1324.7	1.0176	1288.5	1.0281	a++(−)	$(\eta^1\text{-NO})_2$Eu
1335.6	1312.7		1.0174	1276.7	1.0282	a+ −	?
1187.2	1163.9	1187.2, 1163.9	1.0200	1137.7	1.0230	b+(+)	$Eu^+(NO_2)^-$
967.0	950.9	967.1, 950.9	1.0169	924.5	1.0286	a++(−)	$(\eta^2\text{-NO})$Eu site
963.8	947.6	963.9, 947.5	1.0171	921.4	1.0284	a++(−)	$(\eta^2\text{-NO})$Eu
731.9	731.8	731.9	1.0001	694.3	1.0542	a++	$(\eta^2\text{-NO})$EuO
667.8	667.8	667.8	1.0000	633.4	1.0543	a+ −	EuO
657.7	658.1	658.0	0.9994	623.1	1.0562	a+ −(+)	NEuO
494.5	484.0	494.5, 484.0	1.0217	476.1	1.0166	a+ −	Eu(NO)Eu ring

[a] Ratio of $^{14}N^{16}O/^{15}N^{16}O$ isotopic frequencies. [b] Ratio of $^{15}N^{16}O/^{15}N^{18}O$ isotopic frequencies. [c] Annealing behavior: a denotes presence on deposition, +, −, or 0 indicates the direction of growth in two successive annealings, b denotes appearance on the first annealing and +, −, or, 0 indicates changes on second annealing, (+ or −) indicates changes on photolysis, c denotes appearance on photolysis. *Indicates an increase with CCl_4 on deposition. **Indicates a decrease with CCl_4 on deposition.

TABLE 6: Product Absorptions (cm^{-1}) Observed for Laser-Ablated Gd Atoms with NO in Solid Argon

^{14}NO	^{15}NO	$^{14}NO + {}^{15}NO$	ratio[a]	$^{15}N^{16}O + {}^{15}N^{18}O$	ratio[b]	anneal.[c]	ident
1481.2	1453.6	1481.1, 1453.5	1.0190			a++(−)	?
1426.5	1399.2	1426.5, 1399.3	1.0194	1399.1, 1365.8	1.0244	b+(−)	?
1361.6	1338.2	1361.6, 1338.1	1.0175	1338.1, 1301.6	1.0280	a++	?
1187.2	1164.3	1187.3, 1164.2	1.0197	1164.2, 1149.4, 1137.5	1.0235	b+(−)	$Gd^+(NO_2)^-$
1021.7	1005.9	1021.5, 1005.9	1.0157	1005.8, 977.6	1.0289	b+	?
997.6	981.8	997.5, 981.7	1.0161	981.6, 956.4	1.0263	a+0	$(\eta^2\text{-NO})$Gd
844.8	844.8	844.8	1.0000	844.8, 801.3	1.0543	a0−(−)	GdO^+
812.8	812.8	812.8	1.0000	812.8		a− −(−)	GdO
784.3	784.3	784.3	1.0000	784.3, 743.7	1.0546	a+0(+)	$(\eta^2\text{-NO})$GdO
797.1						a+ −	GdN
769.8	769.8	769.8	1.0000	769.8, 729.7	1.0550	a+ −	NGdO
698.5	681.9	698.5, 681.9	1.0243	681.9, 674.0	1.0117	a+ −(+)	?
696.0	678.5	696.0, 678.4	1.0258	678.4, 672.0	1.0095	b+	?
555.9	552.4	555.9, 552.4	1.0063	552.3, 528.7	1.0446	a+ −(+)	Gd(NO)Gd site
544.3	541.0	544.4, 541.1	1.0061	541.0, 517.6	1.0452	a+0(−)	Gd(NO)Gd

[a] Ratio of $^{14}N^{16}O/^{15}N^{16}O$ isotopic frequencies. [b] Ratio of $^{15}N^{16}O/^{15}N^{18}O$ isotopic frequencies. [c] Annealing behavior: a denotes presence on deposition, +, −, or 0 indicates the direction of growth in two successive annealings, b denotes appearance on the first annealing and +, −, or, 0 indicates changes on second annealing, (+ or −) indicates changes on photolysis, c denotes appearance on photolysis. *Indicates an increase with CCl_4 on deposition. **Indicates a decrease with CCl_4 on deposition.

TABLE 7: Product Absorptions (cm^{-1}) Observed for Laser-Ablated Tb Atoms with NO in Solid Argon

^{14}NO	^{15}NO	$^{14}NO + {}^{15}NO$	ratio[a]	$^{15}N^{18}O$	ratio[b]	anneal.[c]	ident
1522.6	1494.3	1522.6, 1494.2	1.0189	1457.0	1.0256	b+	?
1438.8	1416.0	1438.8, 1416.0	1.0161	1380.6	1.0256	a+ −	NTbO combo
1186.8	1164.0	1186.9, 1164.0	1.0196	1137.2	1.0236	b+	$Tb^+(NO_2)^-$
1111.4	1089.6	1111.5, 1089.6	1.0200	1064.3	1.0238	b+(−)	$(\eta^2\text{-NO})$Tb
856.6	856.6	856.6	1.0000	812.3	1.0545	a+ −(−)	TbO^+
823.9	823.9	823.9	1.0000	781.3	1.0545	a− −(−)	TbO
820.2	820.2	820.2	1.0000	777.8	1.0545	a− −	TbO site
816.8	816.8	816.8	1.0000	774.7	1.0543	a− −	TbO site
805.1						a+ −	TbN
793.5	793.5	793.5	1.0000	752.6	1.0543	a+0	$(\eta^2\text{-NO})$TbO
770.6	758.2	770.6, 758.2	1.0164	743.9	1.0192	a+ −	NTbO
763.4	751.4	763.4, 751.4	1.0160	736.8	1.0198	a++(−)	NTbO site
758.6			1.0000	718.5	1.0558	a++	TbO_2 ν_1
756.4			1.0000	716.6	1.0555	b+	$(\eta^1\text{-NO})_x TbO_2$ ν_1
718.6	718.6	718.6	1.0000	683.0	1.0521	a++	TbO_2 ν_3
712.5	712.5	712.5	1.0000	677.2	1.0521	b+	$(\eta^1\text{-NO})_x TbO_2$ ν_3
674.2	663.9	674.2, 663.9	1.0155	641.7	1.0346	a+ −	NTbO
596.0	596.0	596.0	1.0000	566.6	1.0519	a+ −(−)	TbO_3^-
550.3	547.7	550.3, 547.7	1.0047	522.6	1.0480	a++(−)	Tb(NO)Tb

[a] Ratio of $^{14}N^{16}O/^{15}N^{16}O$ isotopic frequencies. [b] Ratio of $^{15}N^{16}O/^{15}N^{18}O$ isotopic frequencies. [c] Annealing behavior: a denotes presence on deposition, +, −, or 0 indicates the direction of growth in two successive annealings, b denotes appearance on the first annealing and +, −, or, 0 indicates changes on second annealing, (+ or −) indicates changes on photolysis, c denotes appearance on photolysis. *Indicates an increase with CCl_4 on deposition. **Indicates a decrease with CCl_4 on deposition.

(reaction 2).

$$\text{Ln} + \text{NO} \rightarrow [\text{NLnO}]^* \rightarrow \text{NLnO or N} + \text{LnO or O} + \text{LnN} \quad (1)$$

$$\text{Ln} + \text{NO} \rightarrow \text{Ln}(\eta^2\text{-NO}); \text{Ln}(\eta^2\text{-NO}) + h\nu \rightarrow \text{NLnO} \quad (2)$$

The anionic species $NCeO^-$ and $NPrO^-$ have also been observed. Unlike the oxide systems, relatively few metal-containing anionic species are formed in the NO experiments because of the high electron affinity of NO_2 present (2.273 ± 0.005 eV),[27] which is a better electron trap than is generally found in the oxides. The determination of the charge is based on results obtained from doping reactant gas mixtures with CCl_4 to capture electrons, thereby minimizing the formation of anions

TABLE 8: Product Absorptions (cm^{-1}) Observed for Laser-Ablated Dy Atoms with NO in Solid Argon

^{14}NO	^{15}NO	$^{14}NO + {}^{15}NO$	ratio[a]	$^{15}N^{18}O$	ratio[b]	anneal.[c]	ident
1523.2	1494.8	1523.1, 1507.5, 1494.9	1.0190	1457.6	1.0255	b+(−)	$(\eta^1\text{-NO})_2\text{Dy}$
1188.0	1165.2	1187.9, 1165.0	1.0196	1138.1	1.0238	b+	$Dy^+(NO_2)^-$
1029.6	1012.9	1029.8, 1012.9	1.0167	984.1	1.0293	b+(−)	?
1023.0	1006.1	1022.8, 1006.1	1.0166	977.7	1.0290	b+(−)	?
888.0	878.0	887.9, 878.0	1.0114	848.9	1.0343	b+(−)	?
861.3	861.3	861.2	1.0000	816.4	1.0550	a+ −(−)	DyO^+
828.7	828.6	828.7	1.0001			a+ −	DyO
825.4	825.4	825.4	1.0000	782.7	1.0546	a− −	DyO site
821.9	822.0	821.9	1.0000	779.4	1.0545	a− −	DyO site
810.5						a+ −	DyN
797.4	797.4	797.4	1.0000	756.4	1.0542	a+ −(+)	$(\eta^2\text{-NO})\text{DyO}$
784.9	784.9	784.9	1.0000	745.2	1.0533	a+ −(+)	NDyO
777.4	777.2	777.3	1.0003			b+	NDyO site
771.4	759.2	771.3, 759.1	1.0161	740.1	1.0257	b+(−)	$(\eta^2\text{-NO})\text{Dy}$
713.7	694.9	713.7, 695.0	1.0271	688.3	1.0096	a+ −(+)	?
702.2	684.8	702.2, 684.4	1.0254	677.6	1.0106	a+ −(−)	?
641.1	632.9	641.1, 632.8	1.0130	626.3	1.0105	b+(−)	$(\eta^2\text{-NO})\text{Dy}$
636.2	620.4	636.2, 620.4	1.0255	614.6	1.0094	a+ −(−)	Dy(NO)Dy ring
576.3	571.2	576.1, 571.2	1.0089	566.0	1.0092	b+	?
550.9	548.7	550.7, 548.7	1.0040	524.0	1.0471	a+ −(−)	Dy(NO)Dy ring

[a] Ratio of $^{14}N^{16}O/^{15}N^{16}O$ isotopic frequencies. [b] Ratio of $^{15}N^{16}O/^{15}N^{18}O$ isotopic frequencies. [c] Annealing behavior: a denotes presence on deposition, +, −, or 0 indicates the direction of growth in two successive annealings, b denotes appearance on the first annealing and +, −, or, 0 indicates changes on second annealing, (+ or −) indicates changes on photolysis, c denotes appearance on photolysis. *Indicates an increase with CCl_4 on deposition. **Indicates a decrease with CCl_4 on deposition.

TABLE 9: Product Absorptions (cm^{-1}) Observed for Laser-Ablated Ho Atoms with NO in Solid Argon

^{14}NO	^{15}NO	$^{14}NO + {}^{15}NO$	ratio[a]	$^{15}N^{16}O + {}^{15}N^{18}O$	ratio[b]	anneal.[c]	ident
1188.6	1165.7	1188.6, 1165.7	1.0196	1165.9, 1150.6, 1139.3	1.0233	b+	$Ho^+(NO_2)^-$
860.7	860.6	860.6	1.0001	860.6, 816.1	1.0545	a− −(−)	HoO^+
828.0	828.0	828.0	1.0000	828.0, 785.1	1.0546	a+ −(−)	HoO
764.7	752.6	764.7, 752.7	1.0161	752.6, 734.2	1.0251	b+(−)	$(\eta^2\text{-NO})\text{Ho}$
724.5	718.3	724.5, 718.3	1.0086	718.3, 695.7	1.0325	a++(+)	NHoO
714.2	696.1	714.2, 696.1	1.0260	- - -, 688.9	1.0105	a++(+)	?
701.8	684.2		1.0257	684.4, 677.7	1.0099	a+ −(−)	?
657.7	654.3	657.7, 654.3	1.0052			a− −(−)	?

[a] Ratio of $^{14}N^{16}O/^{15}N^{16}O$ isotopic frequencies. [b] Ratio of $^{15}N^{16}O/^{15}N^{18}O$ isotopic frequencies. [c] Annealing behavior: a denotes presence on deposition, +, −, or 0 indicates the direction of growth in two successive annealings, b denotes appearance on the first annealing and +, −, or, 0 indicates changes on second annealing, (+ or −) indicates changes on photolysis, c denotes appearance on photolysis. *Indicates an increase with CCl_4 on deposition. **Indicates a decrease with CCl_4 on deposition.

TABLE 10: Product Absorptions (cm^{-1}) Observed for Laser-Ablated Er Atoms with NO in Solid Argon

^{14}NO	^{15}NO	$^{14}NO + {}^{15}NO$	ratio[a]	$^{15}N^{16}O + {}^{15}N^{18}O$	ratio[b]	anneal.[c]	ident
1188.3	1166.0	1188.2, 1166.0	1.0191			b+	$Er^+(NO_2)^-$
984.8	972.3	984.7, 972.2	1.0129			b+	?
	861.8					a− −	ErO^+
	828.5					a+ −	ErO
	824.9					a+ −	ErO site
799.4	799.3	799.4	1.0001	799.4, 758.1	1.0545	a+ −(+)	NErO site
790.3	790.1	790.2	1.0003	790.1, 748.9	1.0550	a+ −(+)	NErO
760.1	748.6	760.0, 748.6	1.0154			b+(−)	$(\eta^2\text{-NO})\text{Er}$
714.3	696.1	714.2, 696.1	1.0261			a+ −(+)	?

[a] Ratio of $^{14}N^{16}O/^{15}N^{16}O$ isotopic frequencies. [b] Ratio of $^{15}N^{16}O/^{15}N^{18}O$ isotopic frequencies. [c] Annealing behavior: a denotes presence on deposition, +, −, or 0 indicates the direction of growth in two successive annealings, b denotes appearance on the first annealing and +, −, or, 0 indicates changes on second annealing, (+ or −) indicates changes on photolysis, c denotes appearance on photolysis. *Indicates an increase with CCl_4 on deposition. **Indicates a decrease with CCl_4 on deposition.

and favoring cations. This technique has successfully supported the identification of the MCO^+ and MCO^- and the $C_2O_4^+$ and $C_2O_4^-$ species, as confirmed by DFT calculations,[28−31] and it has been useful in identifying a range of lanthanide oxide anions and cations.[13]

NLnO Insertion Products. All of the lanthanide and nitric oxide systems provided neutral NLnO insertion products, and two of the systems produced singly charged anions. The NLnO species are identified by the isotopic frequency shifts their fundamental vibrations undergo when $^{15}N^{16}O$, $^{14}N^{16}O + {}^{15}N^{16}O$, and $^{15}N^{18}O$ or $^{15}N^{16}O + {}^{15}N^{18}O$ gas samples are used in place of "plain vanilla" $^{14}N^{16}O$. The number of isotopic peaks provided by the mixed isotope samples is also a key factor in product identification. For an NLnO molecule that contains one N atom and one O atom, the mixed isotopic samples must provide two peaks for each observed fundamental. Product absorptions from the $^{14}N^{16}O$ experiments are provided in the ensuing discussion with $^{15}N^{16}O$ and $^{15}N^{18}O$ isotopic counterparts supplied parenthetically, $^{14}N^{16}O$ ($^{15}N^{16}O$, $^{15}N^{18}O$).

For Ce, Pr, Eu, Gd, Dy, Er, Tm, Yb, and Lu, the vibrational modes of the NLnO product separate into one mostly LnO vibration and one mostly LnN vibration. In those cases for which

TABLE 11: Product Absorptions (cm^{-1}) Observed for Laser-Ablated Tm Atoms with NO in Solid Argon

^{14}NO	^{15}NO	$^{14}NO + {}^{15}NO$	ratio[a]	$^{15}N^{18}O$	ratio[b]	anneal.[c]	ident
1188	1167	1188, 1167	1.0180	1139	1.0246	b+(+)	$Tm^{+}(NO_2)^{-}$
832.0	832.0	832.0	1.0000	788.9	1.0546	a+ −	TmO
803.0	803.0		1.0000	761.2	1.0549	a+ −(+)	(η^2-NO)TmO
795.0	795.9	794.9, 795.9	0.9989	753.8	1.0559	a0−(+)	NTmO

[a] Ratio of $^{14}N^{16}O/^{15}N^{16}O$ isotopic frequencies. [b] Ratio of $^{15}N^{16}O/^{15}N^{18}O$ isotopic frequencies. [c] Annealing behavior: a denotes presence on deposition, +, −, or 0 indicates the direction of growth in two successive annealings, b denotes appearance on the first annealing and +, −, or, 0 indicates changes on second annealing, (+ or −) indicates changes on photolysis, c denotes appearance on photolysis. *Indicates an increase with CCl_4 on deposition. **Indicates a decrease with CCl_4 on deposition.

TABLE 12: Product Absorptions (cm^{-1}) Observed for Laser-Ablated Yb Atoms with NO in Solid Argon

^{14}NO	^{15}NO	$^{14}NO + {}^{15}NO$	ratio[a]	$^{15}N^{18}O$	ratio[b]	anneal.[c]	ident
1193.6	1170.2	1193.7, 1170.2	1.0200	1145.4	1.0217	b+	$Yb^{+}(NO_2)^{-}$
782.0	785.4	782.1, 785.4	0.9957	743.5	1.0564	a0−(+)	NYbO
773.3	773.3	773.3	1.0000	733.3	1.0545	a+ −	?
706.1	688.6	706.1, 688.6	1.0254	681.6	1.0103	a+ −(+)	?
659.9	659.9	659.9	1.0000	625.6	1.0548	a+ −	YbO

[a] Ratio of $^{14}N^{16}O/^{15}N^{16}O$ isotopic frequencies. [b] Ratio of $^{15}N^{16}O/^{15}N^{18}O$ isotopic frequencies. [c] Annealing behavior: a denotes presence on deposition, +, −, or 0 indicates the direction of growth in two successive annealings, b denotes appearance on the first annealing and +, −, or, 0 indicates changes on second annealing, (+ or −) indicates changes on photolysis, c denotes appearance on photolysis. *Indicates an increase with CCl_4 on deposition. **Indicates a decrease with CCl_4 on deposition.

TABLE 13: Product Absorptions (cm^{-1}) Observed for Laser-Ablated Lu Atoms with NO in Solid Argon

^{14}NO	^{15}NO	$^{14}NO + {}^{15}NO$	ratio[a]	$^{15}N^{18}O$	ratio[b]	anneal.[c]	ident
1189.4	1169.5	1189.4, 1169.4	1.0170	1151.9	1.0153	a++	?
946.6	931.9	946.5, 932.0	1.0158			a++	?
929.6	915.4	929.6, 915.4	1.0155			a+0(−)	?
865.1	865.1	865.0	1.0000			a+ −(−)	LuO^{+}
829.4	829.5	829.4	1.0000	786.3	1.0548	a− −	LuO
826.5	826.5	826.4	1.0000	783.4	1.0550	a0−(−)	LuO site
823.6	823.6	823.5	1.0000	780.9	1.0547	a0−	LuO site
819.8	819.8	819.7	1.0000	777.4	1.0545	a0−(−)	LuO site
806.8	806.8	806.8	1.0000	806.8	1.0000	a0−	aggregate
797.2	797.1	797.1	1.0001	755.7	1.0548	a+ −(+)	NLuO
790.9	790.9	790.8	1.0000	749.8	1.0548	a++	NLuO site
626.9	626.9	626.9	1.0000	626.9	1.0000	a+ −(−)**	LuO_2^{-}
572.8	569.4	572.8, 569.4	1.0060	544.4	1.0459	a++(−)	Lu(NO)Lu
425.6	412.5	425.5	1.0318	412.4	1.0002	a+ −(+)	NLuO

[a] Ratio of $^{14}N^{16}O/^{15}N^{16}O$ isotopic frequencies. [b] Ratio of $^{15}N^{16}O/^{15}N^{18}O$ isotopic frequencies. [c] Annealing behavior: a denotes presence on deposition, +, −, or 0 indicates the direction of growth in two successive annealings, b denotes appearance on the first annealing and +, −, or, 0 indicates changes on second annealing, (+ or −) indicates changes on photolysis, c denotes appearance on photolysis. *Indicates an increase with CCl_4 on deposition. **Indicates a decrease with CCl_4 on deposition.

both vibrational fundamentals of the dioxide insertion product have also been identified, Ce, Pr, Dy, Tm, and Yb, the LnO stretch of the NLnO molecule has a higher frequency than the average of the two OLnO frequencies (Table 15). This is explained by the ligand field model; because O is more electronegative than N, it competes more successfully for the valence electrons of the metal, causing an increase in bond strength over the dioxide case, in which O must compete with another O. Except for NYbO, the LnO mode of the NLnO molecules is lower than the frequency of diatomic LnO (Table 15). The aberration for NYbO is due to a greater difference between the electronic configuration of the YbO portion of the molecule and the YbO diatomic, relative to the other NLnO species.

Because the O ligand is more electronegative than the N ligand, the LnO bond of NLnO is satisfied first, with the remaining valence electrons used to bond the N atom. Therefore, the strength of the N bond of NLnO is related to the promotion threshold of the Ln f electrons, which, in turn, regulates the valence electron availability. When the LnN fundamental of the NLnO molecule is observed, it is lower than the molecular LnN vibration, except in the case of Pr, for which the PrN mode of NPrO is even higher than the frequency of the PrN diatomic[15] and is also higher than the PrO mode of NPrO (Table 15). Praseodymium may have a lower promotion threshold for its f electrons than the other lanthanides. According to this model, because Pr has five valence electrons, including its f shell, if both f electrons are involved in bonding, Pr could satisfy both of the N and the O ligands, approximating a triple bond to N and a double bond to O. Ce can promote one f electron into the CeN bond of NCeO, approximating a CeN double bond, and Lu, which has a very stable, complete f shell, should promote none, and so, has the lowest LnN vibration for the NLnO molecule, with only a single bond to N.

Using NCeO as an example, the dominant feature lower than 1000 cm^{-1}, in the spectra of atomic Ce ablated into a condensing argon stream in the presence of NO, occurs at 757.2 (751.9, 727.3) cm^{-1}, doubles after 30 K annealing, and is assigned to the NCeO neutral molecule (Figure 1). Isotopic mixtures of both $^{14}N^{16}O + {}^{15}N^{16}O$ and $^{15}N^{16}O + {}^{15}N^{18}O$ provide doublets for the observed fundamental, demonstrating conclusively that one O atom and one N atom are involved in the vibration. The isotopic shift from ^{14}NO to ^{15}NO is not large, only 5.3 cm^{-1}, and yields an isotopic ratio of 1.0070. The shift of 24.6 cm^{-1} from $^{15}N^{16}O$ to $^{15}N^{18}O$ yields an isotopic ratio of 1.0338 (Table

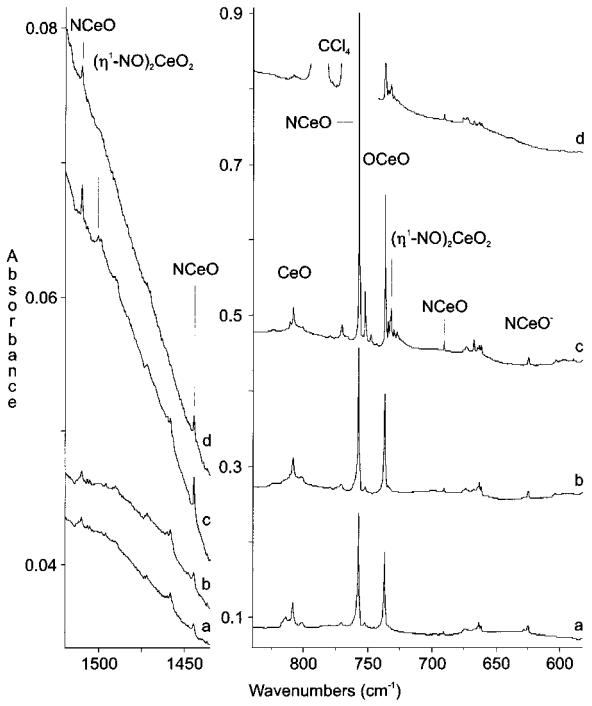

Figure 1. Infrared spectra in the 1520−1435 and 840−580 cm^{-1} regions for laser-ablated cerium atoms co-deposited with $^{14}N^{16}O$/Ar: (a) 0.2% NO/Ar after 50 min dep; (b) 0.2% NO/Ar after Hg-arc photolysis; (c) 0.2% NO/Ar after 30 K annealing; (d) 0.2% NO/0.05% CCl_4/Ar after 30 K annealing.

1), which is approaching the CeO $^{16}O/^{18}O$ isotopic ratio of 1.0536. This allows assessment of the fundamental at 757.2 cm^{-1} as primarily a cerium−oxygen motion.

A much weaker absorption, with about $^1/_{60}$ the intensity of the strong 757.2 cm^{-1} fundamental, occurs at 690.8 (673.9, 661.2) cm^{-1} and mirrors the much stronger band in the variation of its intensity through photolysis and annealing cycles (Figure 1). This parallel tracking behavior allows attribution of both absorptions to the same chemical species. The magnitude of the separation in frequency between the two and the very different isotopic shift ratios preclude assignment as matrix sites; therefore, these absorptions are due to the two vibrational fundamentals of the NCeO molecule. The weaker band has a $^{14}N^{16}O/^{15}N^{16}O$ ratio of 1.0251, approaching 1.0314, the $^{14}N/^{15}N$ isotopic ratio of the CeN molecule, and a $^{15}N^{16}O/^{15}N^{18}O$ ratio of 1.0192, showing that N participates more than O in this fundamental mode.

Additionally, the first overtone of the 757.2 (751.9, 727.3) cm^{-1} fundamental is detected at 1510.2 (1499.1, 1451.0) cm^{-1}, which is 4.2 (4.7, 3.6) cm^{-1} lower than twice the fundamental due to anharmonicity. Also, the combination band resulting from both fundamentals is observed at 1444.4 (1423.7, 1384.6) cm^{-1}, which is 3.6 (2.1, 3.9) cm^{-1} lower than the sum of the fundamentals. These bands also track with the lower bands through annealing and photolysis cycles (Figure 1).

The NCeO fundamentals (757.2, 690.8 cm^{-1}) may be compared with the modes for NLaO (742.2, <400 cm^{-1}) and NHfO (855.2, 685.3 cm^{-1}).[10] Both NLaO and NHfO molecules have metal-oxide frequencies lower than the respective monoxides by 50−100 cm^{-1}, but the much larger separation of the nitride stretches may reflect a difference in order between the LaN and HfN bonds of the NMO molecules. In the NLaO molecule, La, with only three valence electrons, forms only a single bond to the N ligand, while Hf, with four valence electrons, forms a double bond, as indicated by the much higher frequency that is obtained. The NCeO molecule has a CeN fundamental that matches the analogous mode of NHfO and, therefore, also suggests the formation of a double bond to the N ligand, promoting one electron from its f shell.

Density functional calculations (Table 14) of the NCeO molecule support this assignment and describe the mechanics of the motions fairly well, as can be seen by the close approximation of the calculated isotopic ratios to the experimentally observed values. The calculated frequencies are higher than the experimental values, but within 5%, and the intensity difference between the peaks is in the proper sense, although the observed peak area discrepancy is several times larger. The same quantitative agreement has been found for the ADF calculated and observed frequencies of NUO.[32]

The NPrO molecule is unique in these experiments. The most intense product absorption in the Pr + NO reaction system occurs at 900.8 (879.1, 873.0) cm^{-1} (Figure 2). Like its cerium analogue, this peak is assigned to the NPrO insertion product. Mixed $^{14}N^{16}O + {}^{15}N^{16}O$ and $^{15}N^{16}O + {}^{15}N^{18}O$ samples provide isotopic doublets of peaks that clearly lack intermediate components (Table 2). Therefore, this vibration is due to the motion of one N atom and one O atom. The $^{14}N/^{15}N$ and $^{16}O/^{18}O$ isotopic ratios, 1.0247 and 1.0070, respectively, indicate that the observed motion is mostly that of an N atom vibrating against a Pr atom, with little involvement of the O atom.

The next strongest product absorption, at 742.0 (737.0, 703.9) cm^{-1}, is one-third the intensity of the larger peak and is assigned to the PrO fundamental vibration of NPrO (Figure 2). This band shows the same behavior as the stronger peak with photolysis and annealing of argon matrixes and also displays mixed isotopic doublets. The $^{14}N/^{15}N$ ratio of 1.0068 and the $^{16}O/^{18}O$ ratio of 1.0470 show that this fundamental is primarily a PrO motion mixed with a small amount of PrN character. Of the NLnO molecules detailed in this study, only in the case of NPrO is the mostly PrN stretch observed as being more intense and blue-shifted from the PrO stretch. Note that the NTaO molecule also has a TaN mode (967.6 cm^{-1})[11] that is higher than the TaO mode (855.8 cm^{-1})[11] and that Ta has five valence electrons, as does Pr if the two f electrons are involved in bonding. The calculated NPrO singlet state models the vibrational potential of the observed NPrO molecule (Table 14). This is consistent with the proposed bonding structure of the NPrO molecule based on the spectroscopic evidence.

The combination band, observed at 1638.3 (1610.9, 1573.1) cm^{-1}(which is 4.5 (5.2, 3.8) cm^{-1} less than the sum of the two fundamentals due to anharmonic vibrational contributions), corroborates the identity of the two fundamentals of NPrO (Figure 2). The overtone of the primarily PrO fundamental is also weakly observed at 1480.3 (1470.7, 1404.8) cm^{-1}, only 3.7 (3.3, 3.0) cm^{-1} less than twice the fundamental (Figure 2). The behavior of these bands with photolysis and annealing cycles parallels that of the fundamentals of NPrO.

The dominant product absorption in the Nd + NO reaction system occurs at 768.7 (759.9, 740.3) cm^{-1}. This band increases after annealing to 25 K, but is unaffected by Hg-arc photolysis, tracking with a much weaker absorption (9% of the intensity) at 661.4 (648.6, 631.5) cm^{-1}. Both of these bands are attributed to the NNdO molecule. However, the motions of the O and N atoms mix to render two normal modes, neither of which can be assigned to a primarily NdN or NdO vibration on the basis of the isotopic frequency ratios (Table 3). Confirming the association of the two fundamentals is a combination band that absorbs at 1424.1 (1402.9, 1366.3) cm^{-1}, 6.0 (5.6, 5.5) cm^{-1} below the sum (Table 3).

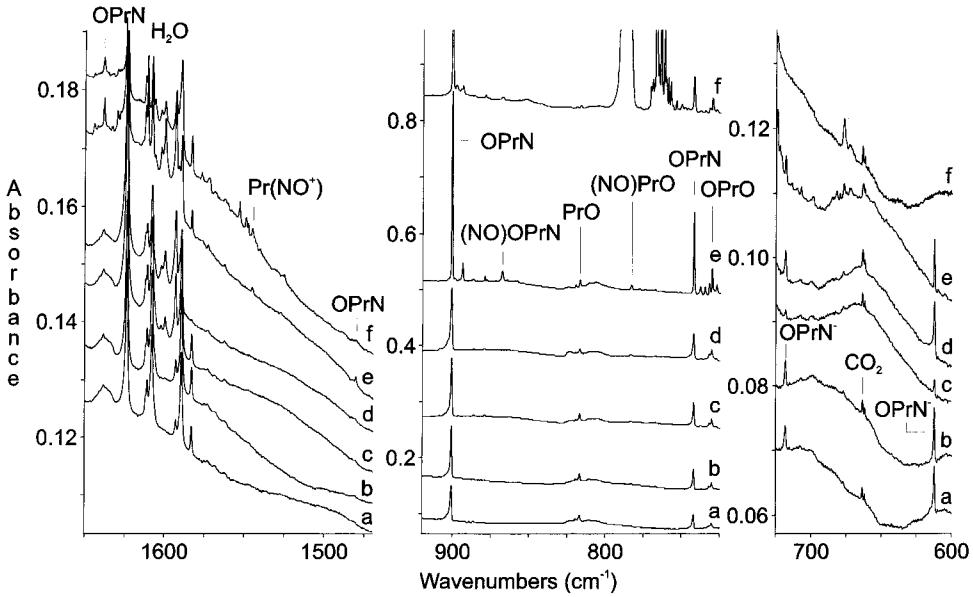

Figure 2. Infrared spectra in the 1650−1470, 920−720, and 725−600 cm^{-1} regions for laser-ablated praseodymium atoms co-deposited with 0.2% $^{14}N^{16}O$/Ar after: (a) 1 h dep; (b) 20 K annealing; (c) tungsten lamp photolysis; (d) Hg-arc photolysis; (e) 30 K annealing; (f) 0.2% $^{14}N^{16}O$/0.05% CCl_4/Ar after 1 h deposition.

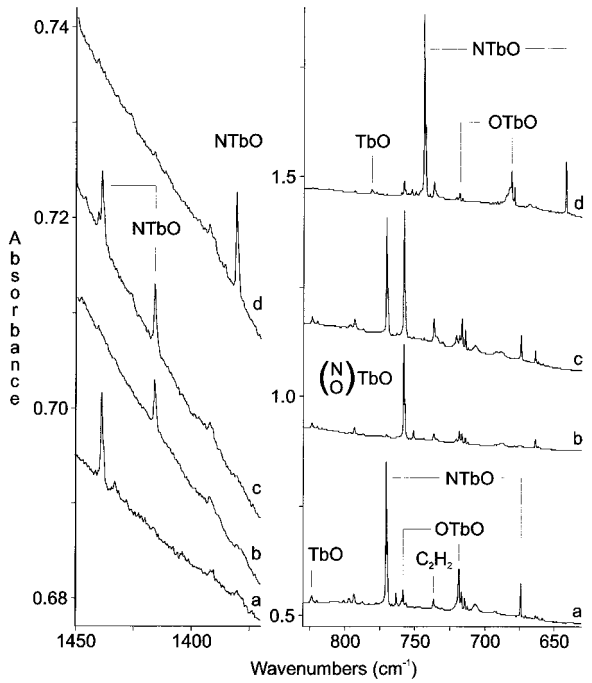

Figure 3. Infrared spectra in the 1450−1370 and 830−630 cm^{-1} regions for laser ablated terbium atoms co-deposited with NO after Hg-arc photolysis: (a) 0.2% $^{14}N^{16}O$/Ar; (b) 0.1% $^{15}N^{16}O$/Ar; (c) 0.3% mixed $^{14}N^{16}O/^{15}N^{16}O$/Ar; (d) 0.2% $^{15}N^{18}O$/Ar.

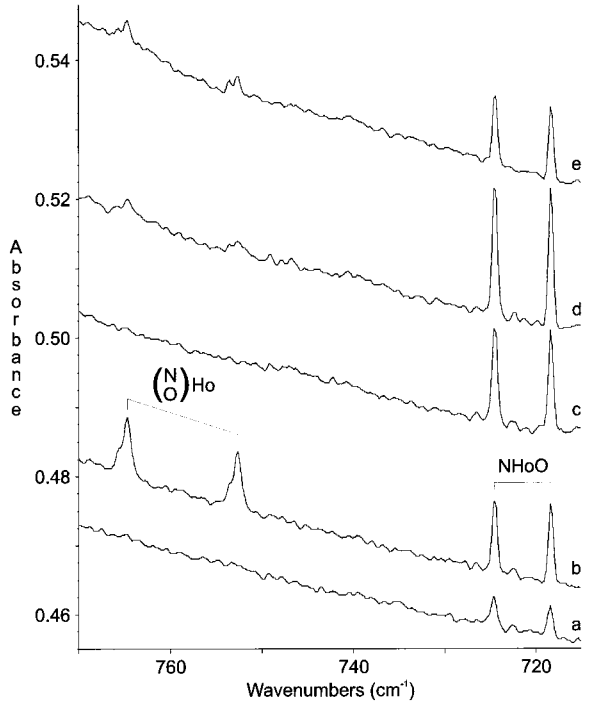

Figure 4. Infrared spectra in the 770−715 cm^{-1} region for laser-ablated holmium atoms co-deposited with 0.3% mixed $^{14}N^{16}O/^{15}N^{16}O$: Ar after: (a) 1 h deposition; (b) 25 K annealing; (c) Hg-arc photolysis; (d) 30 K annealing; (e) 40 K annealing.

Density functional calculations were performed on two low-lying states of NNdO, the doublet and the quartet. The vibrational potential is modeled well by the quartet state, calculated to be 0.4 eV higher in energy, which is within the energy accuracy of the calculation (Table 14). On the other hand, the energetically lower doublet state more closely resembles the NPrO molecule, which promotes two f electrons to bonding orbitals, rather than the NNdO molecule, which promotes just one.

Finally, both the LuO and the LuN fundamentals of NLuO are observed at 797.2 (797.1, 755.7) and 425.6 (412.5, 412.4) cm^{-1}, respectively (Table 13). The two modes track with each other through photolysis and annealing cycles (Figure 6). The observation of precisely diatomic LuO (ratio 1.0548) and LuN (ratio 1.0318) isotopic ratios (Table 13) for the two modes indicates that there is no interaction between the two bond stretching modes for NLuO.

The LuN mode of NLuO is the lowest observed LnN mode of any of the NLnO species. This is because the Lu atom has a very stable f^{14} electron configuration that does not promote any f electrons into the metal valence shell and thus forms a weak bond to the N ligand involving only one valence electron from the metal center. The vibrational potential is modeled

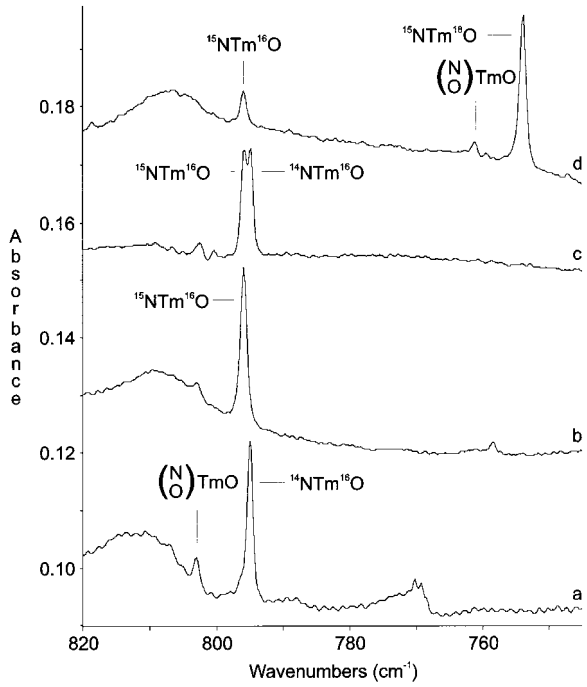

Figure 5. Infrared spectra in the 820−745 cm^{-1} region for laser-ablated thulium atoms co-deposited with: (a) 0.2% $^{14}N^{16}O$/Ar after Hg-arc photolysis; (b) 0.3% $^{15}N^{16}O$/Ar after Hg-arc photolysis; (c) 0.3% mixed $^{14}N^{16}O$/$^{15}N^{16}O$: Ar after 30 K annealing; (d) 0.3% $^{15}N^{18}O$/Ar after Hg-arc photolysis.

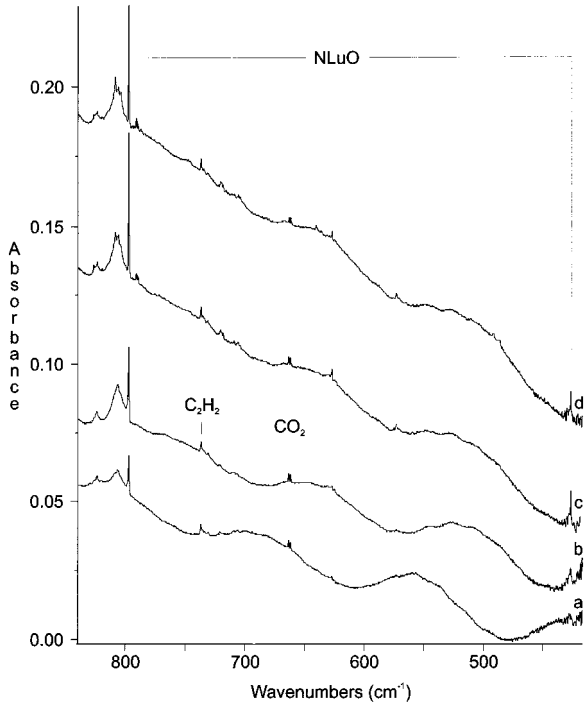

Figure 6. Infrared spectra in the 840−415 cm^{-1} region for laser-ablated lutetium atoms co-deposited with 0.2% $^{14}N^{16}O$/Ar (a) after 1 h deposition; (b) after tungsten lamp photolysis; (c) after 30 K annealing; (d) after 40 K annealing.

particularly well by density functional calculations, which underestimate the observed frequencies by about 10 cm^{-1} (Table 14).

Ln(NO) and OLn(NO) Ring Species. For Eu−Er, absorptions observed from 1120 to 760 cm^{-1} provide mixed NO isotopic doublets of peaks and ratios appropriate for an NO vibrational mode and, therefore, are assigned to the simplest molecule containing a single NO unit, the trigonal ring. The $(NO)^{2-}$ vibrational frequency has been measured for $Li^+(NO)^{2-}Li^+$ at 886 cm^{-1},[33] which provides a frequency region for the trigonal ring NO stretching modes and allows these molecules to be described as $Ln^{2+}(NO)^{2-}$ ion pairs. For those cases in which the inserted NLnO bands increase with photolysis, the Ln(NO) bands are decreased or destroyed and regain intensity with successive annealing (Figure 4). Therefore, the Ln(NO) molecule is identified as an important intermediate in the formation of NLnO. The observed frequencies for the NO stretches of these rings are provided in Tables 5−10. Table 8 provides an additional stretch that tracks with the NO vibration and is assigned to a Dy−(NO) vibration of the Dy(NO) ring.

An LnO stretch found from 730 to 800 cm^{-1} for Ce, Pr, Nd, Eu, Gd, Tb, Dy, and Tm is assigned to the (η^2-NO) ligated LnO species. With the exception of Eu, this diatomic LnO stretch is red-shifted from the isolated monoxide by 30−50 cm^{-1}, which is expected because the O ligand must compete for electron density, after the NO complexation of LnO. In the case of Eu, the 60 cm^{-1} blue shift is explained by the loss of the half-filled f^7 configuration on the metal center upon accommodation of the NO ligand. This removes the circumstance that causes the EuO frequency to be unusually low relative to the other LnO diatomic frequencies, and so, it shifts the EuO frequency in the (NO)EuO complex into the range of the other (NO)LnO diatomic vibrations. The complexed NO ligand is proposed to be side-bound because, in the case of the Ce analogue, an NO vibration at 1145.2 cm^{-1} tracks with the lower CeO mode of the (NO)CeO species; the 1145.2 cm^{-1} vibration is lower than the range for an end-bound NO vibration and, therefore, is due to side-bound ligation. Because the LnO frequencies of the other (NO)LnO species are located in the vicinity of the CeO mode of (NO)CeO, all are proposed to have the same, side-bound, structure.

Ln(NO)Ln Ring Species. One or two fundamentals of the Ln(NO)Ln ring are tentatively assigned for 8 of the 13 lanthanides in this study. The observed modes remain largely unmixed, retaining either the LnO or the LnN vibrational character. These vibrations present isotopic doublets for $^{14}N^{16}O$/$^{15}N^{16}O$ and $^{15}N^{16}O$/$^{15}N^{18}O$ mixtures, indicating the presence of a single NO unit in the absorber, and they are in the same region that the analogous $(LnN)_2$[15] and $(LnO)_2$[13] rings are observed. In most cases, the $(LnN)_2$ ring has been observed at higher frequency than the $(LnO)_2$ ring, and when both modes of the Ln(NO)Ln molecule are assigned, the N motion is higher in frequency than the O motion. Tentative frequencies are provided in Tables 1−3, 5−8, and 13.

$Ln^+(NO_2)^-$. The absorptions observed for $Ln^+NO_2^-$ in the 1200−1180 cm^{-1} region are similar to those of the alkali metal nitrites[34] and the ozonide bands found universally in lanthanide oxide experiments.[13] Broad absorptions form on annealing and increase markedly up to 40 K for the later lanthanides (Sm−Yb). In all instances, an isotopic doublet is clearly observed for the $^{14}N^{16}O$/$^{15}N^{16}O$ mixtures, demonstrating that only one N atom is involved in the stretch. Holmium spectra, taken for a $^{15}N^{16}O$/$^{15}N^{18}O$ mixture, provide an isotopic triplet of peaks, indicative of two O atoms in the complex. The observed band is the ν_3 stretch of the NO_2^- ligand. Isotopic N and O ratios for the terbium product place the angle of the ONO bond at 103 ± 3°.

Nitrosyl Complexes. The cerium and praseodymium systems contain several nitrosyl complexes. Other reaction systems are less prolific with regard to NO ligation and have few complexes, the side-bound oxide complex, (NO)LnO, being the most

TABLE 14: Calculated Parameters (ADF 2.1) for Inserted NLnO Species

molecule	multiplicity angle (deg)	bond length (Å)[a]	energy (eV)	frequency (cm^{-1})	intensity (km/mol)	experimental (cm^{-1})
$^{14}NCe^{16}O$	doublet	1.84, 1.81	−19.71	774, 721, 77	250, 20, 160	757.2, 690.8
$^{15}NCe^{16}O$	180°			766, 706, 76	270, 2, 140	751.9, 673.9
$^{15}NCe^{18}O$				746, 688, 74	210, 40, 140	727.3, 661.2
$^{14}NPr^{16}O$	singlet	1.80, 1.71	−20.32	944, 779, 68	320, 140, 140	900.8, 742.0
$^{15}NPr^{16}O$	180°			920, 775, 67	330, 110, 140	879.1, 737.0
$^{15}NPr^{18}O$				915, 738, 66	290, 130, 140	873.0, 703.9
$^{14}NNd^{16}O$	doublet	1.80, 1.72	−20.26	904, 761, 123	320, 90, 140	768.7, 661.4
$^{15}NNd^{16}O$	180°			883, 754, 121	340, 70, 140	759.9, 648.6
$^{15}NNd^{18}O$				875, 721, 119	290, 90, 140	740.3, 631.5
$^{14}NNd^{16}O$	quartet	1.81, 1.77	−19.86	808, 716, 161	250, 30, 120	768.7, 661.4
$^{15}NNd^{16}O$	180°			798, 703, 159	270, 10, 120	759.9, 648.6
$^{15}NNd^{18}O$				779, 683, 155	220, 40, 120	740.3, 631.5
$^{14}NGd^{16}O$	dectet	1.84, 2.12	−24.90	775, 478, 91	140, 40, 10	769.8
$^{15}NGd^{16}O$	180°			775, 464, 91	140, 30, 10	769.8
$^{15}NGd^{18}O$				735, 463, 86	120, 30, 10	729.7
$^{14}NTb^{16}O$	heptet	1.82, 1.76	−20.64	806, 702, 134	250, 30, 160	770.6, 674.2
$^{15}NTb^{16}O$	180°			793, 690, 132	260, 10, 160	758.2, 663.9
$^{15}NTb^{18}O$				777, 668, 129	220, 30, 160	743.9, 641.7
$^{14}NLu^{16}O$	triplet	1.82, 2.18	−14.68	788, 418, 143	90, 10, 10	797.2, 425.6
$^{15}NLu^{16}O$	104°			788, 405, 141	90, 10, 10	797.1, 412.5
$^{15}NLu^{18}O$				746, 405, 136	80, 10, 10	755.7, 412.4

[a] LnO first, LnN second.

TABLE 15: Comparison of Argon Matrix Frequencies (cm^{-1}) for LnO_2, NLnO, LnO, and LnN

Ln	LnO_2[a]		NLnO[b]		LnO	NLnO[c]		LnN
Ce	747.0	<	757.2	<	808.3	690.8	<	843.3
Pr	713 ± 5[d]	<	742.0	<	816.9	900.8	>	857.9
Nd	689 ± 5[d]	<	768.7[e]	<	814.2	661.4[e]	<	853.3
Sm	623 ± 5[d]	<	736.9[e]	<	807.4			822.6
Eu			657.8	<	667.8			820 ± 10[f]
Gd			769.8	<	812.7			797.0
Tb	739	<	770.6[e]	<	823.9	674.2[e]	<	805.3
Dy	597 ± 5[d]	<	784.9	<	829.0			810.5
Ho	599.0	<	724.5	<	828.1			805 ± 10[f]
Er			790.3	<	828.5			800 ± 10[f]
Tm	661.2	<	795.0	<	832.0			805 ± 10[f]
Yb	630 ± 5[d]	<	782.0	>	660.0			770 ± 10[f]
Lu			797.2	<	829.3	425.6	<	800 ± 10[f]

[a] Average is $(\nu_1 + \nu_3)/2$. [b] Mostly LnO vibration. [c] Mostly LnN vibration. [d] ν_1 used in average is estimated from $\nu_1 + \nu_3$. [e] LnN and LnO modes of NLnO are heavily mixed. [f] LnN in argon is estimated from LnN in N_2.

common (Figures 2, 3, and 5). Several of the cerium nitrosyl species are discussed below, and all identified complexes are provided in Tables 1−13.

Both the mono- and dinitrosyl of atomic cerium are identified in Table 1. Additionally, an NO vibration 100 cm^{-1} higher than that of the cerium dinitrosyl, also containing two equivalent end-bound NO subunits, tracks with a perturbed CeO_2 band that appears on the first annealing and continues to increase with successive annealings, providing assignments for both the CeO_2 (ν_3) and the NO vibrational frequencies of $(NO)_2CeO_2$. Lower than the NO vibration of the (NO)CeO species previously discussed is an NO peak at 1078.7 (1061.1, 1031.3) cm^{-1} which arises from two equivalent side-bound NO subunits, based on a triplet mixed isotopic spectrum. As is expected, the side-bound NO ligands associate more strongly with the metal center and thus have weaker NO bonds and lower vibrational frequencies.

NO units bound to the dioxide compete poorly as ligands with the more electronegative O atoms and have the highest frequencies, followed by the dinitrosyl and the mononitrosyl. Because O is a better ligand than NO, the NO bond in the (NO)CeO species is stronger than the NO bond in the side-bound $Ce(NO)_2$ complex and thus has a higher frequency.

Conclusions

Thirteen NLnO molecules are characterized for the first time in matrix isolation infrared experiments. Vibrational motions of these species tend to involve either the O atom or the N atom and the metal center, although for NNdO, NSmO, and NTmO, the two modes are mixed heavily. For the NLnO molecules in which the N and O motions remain separate, the LnO stretch of the NLnO molecule lies between the average LnO frequency in the OLnO molecule and the LnO frequency of the diatomic molecule.[13] The LnN stretch is observed mostly unmixed with LnO in three cases, NPrO, NCeO, and NLuO, in three very different positions, 900.8, 690.8, and 425.6 cm^{-1}, respectively. This behavior is ascribed to the higher electronegativity of O compared to that of N. In competition for valence electrons on the metal, O gains more electron density when it competes with N than when it competes with another O. This pushes the O vibrational frequency higher relative to OLnO, but the N ligand, which must bind with the remaining electrons after the O ligand has been satisfied, varies widely in frequency and provides a clue to the electronic state of the molecule.

In the case of Pr, the PrN stretch of NPrO at 900.8 cm^{-1} is 40 cm^{-1} higher than that of diatomic PrN,[15] which is consistent with promotion of two f electrons of Pr to bonding orbitals of the NPrO molecule. Because no nonbonding valence electrons remain on the Pr metal center to interfere with the electrostatic attraction between the metal center and the N atom, the N is bound even more tightly in the NPrO molecule than in the PrN diatomic.

In NCeO, the CeN stretch at 690.8 cm^{-1} is 150 cm^{-1} lower than the frequency of the CeN diatomic,[15] which is presumed to approximate a CeN triple bond. Therefore, the CeN bond of NCeO is, approximately, a double bond, which suggests that the Ce f electron has been moved into an NCeO bonding orbital. The highly mixed modes for NNdO and NTbO, found at 661.4 and 674.2 cm^{-1}, respectively, suggest that these molecules also involve the promotion of a single f electron into a bonding orbital of the inserted molecule.

NLuO has an LuN frequency at 425.6 cm^{-1}, which is 375

cm^{-1} lower than the frequency of the LuN diatomic.[15] This suggests that the Lu metal center in NLuO is trivalent and does not promote any f electrons to bonding orbitals, approximating an LuN single bond in the NLuO molecule. This behavior is due to the enhanced stability of the completed f^{14} shell on the Lu atom and is postulated to hold for the NGdO molecule as well, which probably maintains a stable f^7 half-filled configuration on the Gd atom, leaving only three valence electrons for bonding. Collectively, these observations allow prediction of the frequencies of LnN single bonds at 420 cm^{-1}, double bonds at 690 cm^{-1}, and triple bonds at 900 cm^{-1}.

The side-bound Ln(NO) molecule proves to be an important intermediate in one formation mechanism of the NLnO insertion product. This trigonal ring increases with annealing, demonstrating that it does not require activation energy to form. Ultraviolet photolysis of the ring causes the metal atom to insert into the weakened NO bond, increasing the yield of NLnO.

Acknowledgment. We gratefully acknowledge N.S.F. support for this research under Grant No. CHE 97-00116.

References and Notes

(1) Peters, M. S.; Jen, L. W. *Atmos.Environ.* **1977**, *11*, 459.
(2) Parvulescu, V. I.; Grange, P.; Delmon, B. *J. Phys. Chem. B* **1997**, *101*, 6933.
(3) Fernandezgarcia, M.; Rebollo, E. G.; Ruiz, A. G.; Conesa, J. C.; Soria, J. *J. Catal.* **1997**, *172*, 146.
(4) Zhang, Y.; Flytzani-Stephanopoulos, M. *J. Catal.* **1996**, *164*, 131.
(5) Ferri, D.; Forni, L.; Dekkers, M. A. P.; Nieuwenhuys, B. E. *Appl. Catal., B***1998**, *16*, 339.
(6) Li, Z. J.; Flytzani-Stephanopoulos, M. *Appl. Catal., A* **1997**, *165*, 15.
(7) Schulze, P. D.; Hardegree, E. L. *J. Phys. Chem.* **1989**, *93*, 5254.
(8) Kushto, G. P.; Zhou, M.; Andrews, L.; Bauschlicher, C. W., Jr. *J. Phys. Chem. A* **1999**, *103*, 1115.
(9) Zhou, M. F.; Andrews, L. *J. Phys. Chem. A* **1999**, *103*, 478.
(10) Kushto, G. P.; Andrews, L. *J. Phys. Chem. A* **1999**, *103*, 4836. Andrews, L.; Liang, B.; Zhou, M. F. 1999, unpublished results (La with NO).
(11) Zhou, M. F.; Andrews, L. *J. Phys. Chem. A* **1998**, *102*, 10025.
(12) Field, R. W. *Ber. Bunsen-Ges. Phys. Chem.* **1982**, *86*, 771.
(13) Willson, S. P.; Andrews, L. *J. Phys. Chem. A* **1999**, *103*, 3171. Willson, S. P.; Andrews, L. *J. Phys. Chem. A* **1999**, *103*, 6972.
(14) Dolg, M.; Stoll, H. *Theor. Chim. Acta* **1989**, *75*, 369.
(15) Willson, S. P.; Andrews, L. *J. Phys. Chem A* 1998, *102*, 10238. Willson, S. P.; Andrews, L. *J. Phys. Chem A* **1999**, *103*, 1311.
(16) Burkholder, T. R.; Andrews, L. *J. Chem. Phys.* 1991, *95*, 8697. Hassanzadeh, P.; Andrews, L. *J. Phys. Chem.* **1992**, *96*, 9177.
(17) Zhou, M. F.; Andrews, L. *J. Phys. Chem. A* **1998**, *102*, 7452.
(18) Andrews, L.; Zhou, M. F.; Willson, S. P.; Kushto, G. P.; Snis, A.; Panas, I. *J. Chem. Phys.* **1998**, *109*, 177 and references therein.
(19) *ADF 2.1, Theoretical Chemistry*; Vrije Universiteit: Amsterdam.
(20) Baerends, E. J.; Ellis, D. E.; Ros, P. *Chem. Phys.* **1973**, *2*, 41.
(21) teVelde, G.; Baerends, E. J. *Comput. Phys. Commun.* **1992**, *99*, 84.
(22) Vosko, S. H.; Wilk, L.; Nusair, M. *Can. J. Phys.* **1980**, *58*, 1200.
(23) Becke, A. D. *Phys. Rev. A: At., Mol., Opt. Phys.* **1988**, *38*, 3098.
(24) Perdew, J. P. *Phys. Rev. B: Condens. Matter* **1986**, *33*, 8822.
(25) Ziegler, T. Ph.D. Thesis, Vrije Universiteit, Amsterdam, 1987.
(26) Heinemann, C.; Cornehl, H. H.; Scroder, D.; Dolg, M.; Schwarz, S. *Inorg. Chem.* **1996**, *35*, 2463.
(27) Ervin, K. M.; Ho, J.; Lineberger, W. C. *J. Phys. Chem.* **1988**, *92*, 5405.
(28) Zhou, M. F.; Andrews, L. *J. Chem. Phys.* **1998**, *109*, 10893.
(29) Zhou, M. F.; Andrews, L. *J. Am. Chem. Soc.* **1998**, *120*, 11499.
(30) Zhou, M. F.; Andrews, L. *J. Phys. Chem. A* **1998**, *102*, 10250.
(31) Zhou, M. F.; Andrews, L. *J. Chem. Phys.* **1999**, *110*, 2414 and 6820.
(32) Kushto, G. P.; Souter, P. F.; Andrews, L.; Neurock, M. *J. Chem. Phys.* **1997**, *14*, 5894.
(33) Tevault, D. E.; Andrews, L. *J. Phys. Chem.* **1973**, *77*, 1640.
(34) Milligan, D. E.; Jacox, M. E. *J. Chem. Phys.* **1971**, *55*, 3404.